Characterization of $Al_xGa_{1-x}As$/GaAs heterojunction bipolar transistor structures using cross-sectional scanning force microscopy

P. A. Rosenthal and E. T. Yu[a)]
Department of Electrical and Computer Engineering and Graduate Program in Materials Science, University of California San Diego, La Jolla, California 92093-0407

R. L. Pierson and P. J. Zampardi[b)]
Rockwell International Science Center, 1049 Camino Dos Rios, Thousand Oaks, California 91358

(Received 29 July 1999; accepted for publication 28 October 1999)

We have characterized base-layer width and dopant distributions on cleaved cross-sections of $Al_xGa_{1-x}As$/GaAs heterojunction bipolar transistor (HBT) structures using a variation of electrostatic force microscopy. The contrast observed is sensitive to the local dopant concentration through variations in the depletion layer depth extending into the sample surface, and enables delineation of individual device regions within the epitaxial layer structure with nanoscale spatial resolution. In two epitaxially grown HBT structures, one with 50 nm base width and the other with 120 nm base width, we are able to delineate clearly the emitter, base, collector, and subcollector regions, and to distinguish regions within the collector differing in dopant concentration by a factor of two. We have also distinguished clearly between the base widths in these samples and have precisely measured the difference to be 63 ± 3 nm, in excellent agreement with the nominal difference of 70 ± 7 nm. © *2000 American Institute of Physics.* [S0021-8979(00)00804-5]

I. INTRODUCTION

Materials characterization at or near the nanometer scale remains a significant challenge in the development of epitaxially grown III–V compound semiconductor device structures. Accurate determination of layer thickness, chemical composition, and dopant distributions is essential for analysis and optimization of device performance. In recent years, scanning probe techniques such as electrostatic force microscopy (EFM), scanning Kelvin probe force microscopy (SKPM), and scanning capacitance microscopy (SCM) have emerged as powerful tools for nanoscale characterization of electronic properties in materials and devices. These techniques have become powerful complements, and offer numerous advantages in comparison, to techniques conventionally used for semiconductor device metrology. Many scanning probe measurements may be performed in ambient air at room temperature, resulting in relative ease of use. Additionally, they can overcome spatial resolution limitations of techniques such as secondary ion mass spectrometry and spreading resistance profiling, particularly in the lateral dimension, and circumvent sample preparation requirements of transmission electron microscopy.

The ability to measure directly, using these and other scanning probe techniques, the electrostatic interaction between the probe tip and the sample surface with nanoscale spatial resolution has afforded increased understanding of structural and electronic properties in a wide range of heterostructure materials and devices. SKPM has, for example, been used to characterize potential variations in AlGaAs/InGaAs/GaAs heterostructures[1] and GaAs transistors[2] under applied bias, and has been applied to perform two-dimensional dopant profiling in Si $p-n$ junctions.[3] Surface defects in GaAs/Ge thin films have been investigated using EFM,[4] and layer thickness metrology has been performed using a combination of selective etching and conventional atomic force microscopy (AFM) on cleaved $Al_{0.5}Ga_{0.5}As$/GaAs epitaxial heterostructures.[5]

Characterization of electronic properties using these techniques typically relies upon the electrostatic interaction between the sample and a conducting probe tip. When a bias voltage with both dc and ac components is applied between an electrically conductive probe tip and grounded sample surface, the resulting electrostatic force has spectral components at dc and at frequencies of ω and 2ω, where ω is the applied excitation frequency.[3] The force components at frequencies ω and 2ω are proportional to the capacitance gradient $(\partial C/\partial z)$ between tip and sample. SKPM utilizes the force component at frequency ω to detect variations in surface potential.[3] Several researchers have utilized the force component at frequency 2ω (with varying nomenclature) to probe local electronic properties. Abraham *et al.* refer to this imaging mode as capacitive force microscopy, and have used it to detect the presence of a dielectric layer on Si,[6] and for dopant profiling in Si.[7] More recently, Hochwitz *et al.* used this force component to image dopant profiles in Si integrated circuits, referring to their studies as C' imaging.[8] Xu and Hsu, in studies of surface defects in GaAs/Ge thin films, have referred to data of this type and the images obtained as capacitance gradient images.[4]

In this study, we have used a variation of the standard EFM technique in which the amplitude of the scanning probe tip is detected as it oscillates in response to the electrostatic

a)Electronic mail: ety@ece.ucsd.edu
b)Current address: IBM Microelectronics Division, 1000 River Road M/S 861A, Essex Junction, VT 05452.

 © 2000 American Institute of Physics

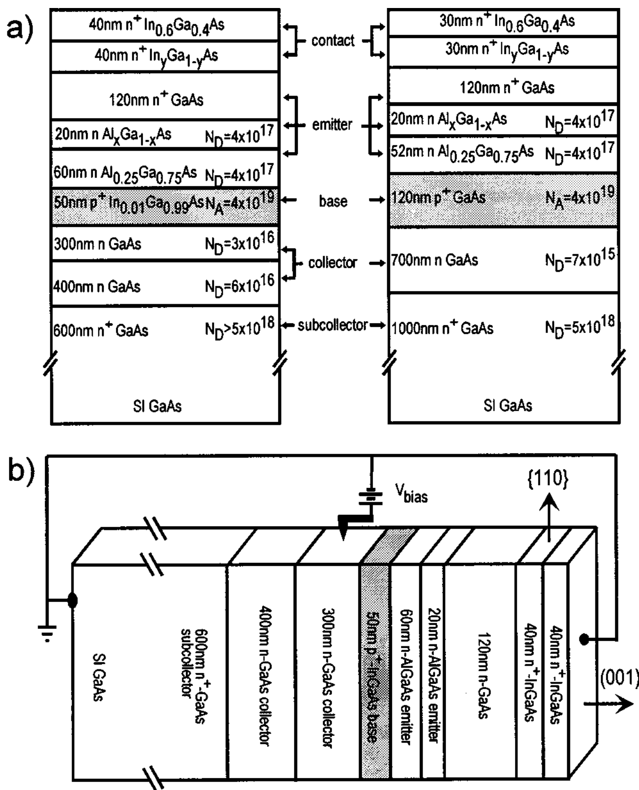

FIG. 1. (a) Schematic diagram of the two HBT epitaxial layer structures investigated, one structure with 50 nm base width and the other with 120 nm base width. All layer widths and dopant concentrations (given in cm^{-3}) are within $\pm 5\%$. (b) Schematic diagram of the cross-sectional geometry used in capacitive force imaging.

force component at frequency 2ω, and therefore refer to this technique as capacitive force imaging. We find that the amplitude contrast in capacitive force imaging is dependent on the bias voltage and the local dopant concentration through the dependence of the depletion layer depth below the sample surface on these quantities, provided that the applied bias is sufficient to unpin the Fermi level at the cleaved surface. We have used capacitive force imaging to characterize the structural and electronic properties of cleaved cross-sections of $Al_xGa_{1-x}As/GaAs$ epitaxial layer heterojunction bipolar transistor (HBT) structures. We have investigated two HBT structures, one with 50 nm base width and one with 120 nm base width. Monitoring the variation in oscillation amplitude during scanning yields contrast which allows us to clearly identify device layers, to distinguish between regions of differing dopant concentration, and to precisely determine the difference in base width between the two HBT samples.

II. SAMPLES AND MEASUREMENT TECHNIQUE

The HBT structures used in this study were grown by metal organic chemical vapor deposition on semi-insulating (SI) GaAs (001) substrates. Figure 1(a) shows a schematic diagram of the two epitaxial layer structures employed, including the individual layer thicknesses, composition, and dopant type and concentration. The emitter, base, collector, and subcollector layers are identified in each structure. Figure 1(b) shows a schematic representation of the cross-sectional geometry used in our experiments, including the orientation and electrical connection of the probe tip with respect to the sample surface. Cross-sectional {110} surfaces were prepared by cleaving the samples in air just prior to imaging.

A Digital Instruments Nanoscope® IIIa MultiMode™ scanning probe microscope system[9] was used to perform surface topographic measurements and capacitive force imaging. The probes consisted of heavily doped *p*-type Si cantilevers onto which ~100 Å Pt was deposited by electron-beam evaporation. Surface topography and capacitive force imaging data were obtained sequentially, using LiftMode™ imaging: first, each topographic line scan was obtained using TappingMode™ atomic force imaging; capacitive force data were then obtained with the tip raised a predetermined distance (referred to hereafter as lift height) above the surface and following the previously measured topographic line profile while scanning. The individual lines of both topographic and capacitive force data obtained in this manner are then combined to produce complete images of each respective data type.

In general, EFM and SKPM data are obtained with a dc and ac bias voltage, $V_{bias}=V_{dc}+V_{ac}\sin\omega t$, applied between the tip and sample. The total potential difference between tip and sample is then $V=(\Delta\Phi/q)+V_{bias}=V_{dc}+(\Delta\Phi/q)+V_{ac}\sin\omega t$, where $\Delta\Phi\equiv\Phi_{sample}-\Phi_{tip}$ is the difference in work function between tip and sample, q is the electron charge, and ω is the applied excitation frequency which is tuned to a resonant frequency of the cantilever—approximately 230 kHz in these studies. This results in an electrostatic force between tip and sample given by[10]

$$F=\frac{1}{2}\left(\frac{\partial C}{\partial z}\right)V^2, \tag{1}$$

where C is the tip–sample capacitance and z the tip–sample separation. In scanning probe techniques such as EFM and SKPM, in which an ac bias is applied near a resonance frequency of the cantilever, changes in cantilever resonant frequency due to the presence of a tip–sample electrostatic force gradient dF/dz lead to corresponding changes in the amplitude of oscillation at the excitation frequency.[11] These techniques are therefore sensitive to the vertical electrostatic force gradient dF/dz, rather than directly to the electrostatic force itself. From Eq. (1) we see that dF/dz is given simply by

$$\left(\frac{dF}{dz}\right)=\frac{1}{2}\left(\frac{\partial^2 C}{\partial z^2}\right)V^2. \tag{2}$$

Substitution of the total potential difference V between sample and probe tip into Eq. (2) yields

$$\left(\frac{dF}{dz}\right)=\left(\frac{dF}{dz}\right)_{dc}+\left(\frac{dF}{dz}\right)_{\omega}+\left(\frac{dF}{dz}\right)_{2\omega} \tag{3}$$

with spectral components at dc and at frequencies ω and 2ω given by[2,3]

$$\left(\frac{dF}{dz}\right)_{\mathrm{dc}}=\frac{1}{2}\left(\frac{\partial^2 C}{\partial z^2}\right)\left[\left(V_{\mathrm{dc}}+\frac{\Delta\Phi}{q}\right)^2+\frac{1}{2}V_{\mathrm{ac}}^2\right], \tag{4}$$

$$\left(\frac{dF}{dz}\right)_{\omega}=\left(\frac{\partial^2 C}{\partial z^2}\right)\left(V_{\mathrm{dc}}+\frac{\Delta\Phi}{q}\right)V_{\mathrm{ac}}\sin(\omega t), \tag{5}$$

$$\left(\frac{dF}{dz}\right)_{2\omega}=-\frac{1}{4}\left(\frac{\partial^2 C}{\partial z^2}\right)V_{\mathrm{ac}}^2\cos(2\omega t). \tag{6}$$

The SKPM technique utilizes the electrostatic force component at frequency ω with a feedback loop adjusting V_{dc} to a value such that $(dF/dz)_{\omega}=0$. From Eq. (5) we see that measurement of V_{dc} will yield a map of local variations in surface potential across a sample surface. In our studies we have utilized primarily the electrostatic force component at frequency 2ω. Specifically, an ac bias voltage, $V_{\mathrm{bias}}=V_{\mathrm{ac}}\sin\omega t$, is applied at a frequency equal to one-half the cantilever resonant frequency with the force component at frequency 2ω therefore being at the resonant frequency of the cantilever. V_{dc} is negligibly small in these measurements. The resulting amplitude contrast then arises through the dependence of $(\partial^2 C/\partial z^2)$ on the bias voltage via the variation in depletion layer depth extending below the sample surface, which in turn is dependent on the local surface state density and dopant concentration in the sample. The cleaved cross-sectional surfaces of our samples are likely to be pinned,[12] and to remain so for small applied tip–sample bias voltages. However, if the applied bias voltage is sufficiently large, and the ac modulation frequency—approximately 115 kHz in our measurements—is sufficiently low that the surface charge has time to respond, the surface Fermi level will be unpinned and the sample surface will alternately undergo accumulation and depletion as the bias voltage oscillates. The signal obtained is the root-mean-square (rms) amplitude of the cantilever oscillation as the cantilever responds to variations in the force component at frequency 2ω.

The basic dependence of $(\partial^2 C/\partial z^2)$, and consequently of this amplitude signal, on the local dopant concentration in the sample can be understood using a relatively straight forward one-dimensional analysis. While we recognize recent work to quantify SCM[13,14] and SKPM[15] data utilizing a two-dimensional analysis, we find that a one-dimensional approach is sufficient to qualitatively explain the observed capacitive force data. There are two components of the capacitance between the conducting tip and sample surface—the capacitance of the gap between tip and sample, C_g, and the depletion layer capacitance C_d. The gap capacitance per unit area is given by $C_g=\epsilon_0/z$, where ϵ_0 is the permittivity of free space. If the applied bias is such that the total potential difference V exceeds the threshold voltage V_{th} necessary to unpin the surface Fermi level (discussed in greater detail in Sec. III), there will exist a depletion layer capacitance per unit area given by $C_d=\epsilon_s/W$, where ϵ_s is the dielectric constant of the semiconductor and W the depletion layer depth extending below the surface. The total capacitance per unit area is then given by

$$C=\frac{\epsilon_0\epsilon_s}{z\epsilon_s+W\epsilon_0}, \tag{7}$$

$$\frac{\partial^2 C}{\partial z^2}=\frac{2\epsilon_0\epsilon_s^3}{(z\epsilon_s+W\epsilon_0)^3}. \tag{8}$$

An n-type (p-type) semiconductor layer will undergo accumulation (depletion) during the positive portion of the ac voltage cycle, i.e., $V_{\mathrm{ac}}\sin\omega t > V_{\mathrm{th}}-(V_{\mathrm{dc}}+\Delta\Phi/q)$, and will be in depletion (accumulation) during the negative portion of the ac voltage cycle, i.e., $V_{\mathrm{ac}}\sin\omega t < -(V_{\mathrm{th}}+V_{\mathrm{dc}}+\Delta\Phi/q)$.[16] During accumulation, the depletion layer width W goes to zero, and the total capacitance per unit area C is simply equal to C_g, and $\partial^2 C/\partial z^2=2\epsilon_0/z^3$, independent of the local dopant concentration. During depletion however, W (for an n-type layer) is given by

$$W=\sqrt{\frac{2\epsilon_s(V_{\mathrm{bi}}+V_d)}{qN_D}}, \tag{9}$$

where V_{bi} is the built-in potential difference corresponding to the surface Fermi-level pinning energy, V_d is the potential drop across the surface depletion region, and N_D is the net donor concentration. A corresponding equation for W for a p-type layer may be obtained by substituting the appropriate values for V_{bi} and V_d, and replacing N_D with the net acceptor concentration N_A. As V_{ac} is increased, the surface eventually undergoes inversion and the depletion layer width W reaches a maximum, unless deep depletion occurs.[16]

From Eqs. (6), (8), and (9) we may deduce that higher doping in a device layer will yield a smaller depletion layer depth W, and consequently a larger value for $(\partial^2 C/\partial z^2)$, a larger force component at frequency 2ω, and a greater amplitude of oscillation at frequency 2ω compared to a device layer with lower doping concentration. This mode of imaging therefore offers the ability to probe, with varying degrees of sensitivity, local differences in dopant concentration and any other aspect of electronic structure on which the total tip–sample capacitance depends.

III. RESULTS

Figure 2(a) shows a cross-sectional topographic profile, averaged over 125 individual line scans, of the 50 nm base HBT structure. Our topographic images regularly exhibit a surface feature, parallel to the epitaxial layer interfaces across the entire topographic image, near the top edge of the cross-sectional samples (right-hand side of Fig. 2). Based on its width and location, we interpret this feature as the $Al_xGa_{1-x}As$ emitter layer, which provides a spatial reference point for analysis of the capacitive force images. Upon cleaving and exposure to ambient air the $Al_xGa_{1-x}As$ emitter layer oxidizes,[17] giving rise to the surface feature exhibited in Fig. 2(a). Figure 2(b) shows a surface plot of the capacitive force data for the 50 nm base sample. The image area is $2.5\ \mu m \times 2.5\ \mu m$ and the data were obtained at a bias $V_{\mathrm{ac}}=2.6$ V and a lift height of 20 nm.

As indicated in Fig. 2(b), the emitter, base, collector, subcollector, and substrate regions can clearly be distinguished in the capacitive force image. The heavily doped base layer appears as a region of higher amplitude than the surrounding, more lightly doped emitter and collector layers, as expected based on the analysis of Sec. II. Similarly, the

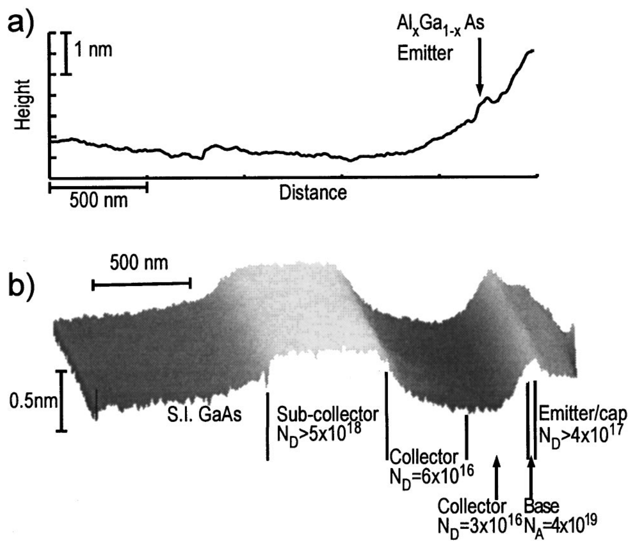

FIG. 2. (a) Topographic profile and (b) 2.5 μm×2.5 μm surface plot of capacitive force data for the 50 nm base HBT structure. A surface feature associated with the oxidized $Al_xGa_{1-x}As$ emitter layer is visible in (a). In (b), the device layers are clearly delineated with the amplitude contrast observed arising from variations in the local dopant concentration (given in cm^{-3}).

n-GaAs collector layers ($N_D=3-6\times10^{16}\,cm^{-3}$) are readily distinguished from the more heavily doped n-GaAs subcollector layer ($N_D>5\times10^{18}\,cm^{-3}$) due to the large difference in oscillation amplitude measured between these regions. This contrast (amplitude difference) demonstrates the ability, using capacitive force imaging, to distinguish between n-type GaAs layers with different dopant concentration, which may provide a precise method for performing layer thickness metrology based on variations in local electronic properties. As mentioned previously, layer thickness metrology has been performed using selective etching followed by conventional AFM on cleaved $Al_{0.5}Ga_{0.5}As$/GaAs epitaxial heterostructures.[5] However, this technique is limited to material systems where appropriate selective etches either exist or can be produced, and is constrained by reproducibility and reliability issues. In addition, it has not been demonstrated that selective etching followed by AFM can be used to distinguish between n-type GaAs layers with different dopant concentration, as are present, for example, between the collector and subcollector regions of the specific HBT structures used in these studies.

Closer examination of the collector region in Fig. 2(b) reveals a change in contrast between the two collector layers arising from their difference in dopant concentration. The collector layer with $N_D=6\times10^{16}\,cm^{-3}$ exhibits higher rms amplitude than the collector layer with $N_D=3\times10^{16}\,cm^{-3}$, consistent with the contrast expected for a more highly doped layer. This contrast demonstrates sensitivity of the capacitive force imaging technique to a factor of two change in local dopant concentration. This level of sensitivity compares well with that reported for other techniques under investigation for dopant concentration profiling, such as scanning capacitance microscopy[18,19] and nanospreading resistance profiling.[20] Neubauer *et al.*[18] report, for example, a 15% change in SCM signal over the concentration range from $N_D=10^{16}$ to $10^{17}\,cm^{-3}$ in studies of implanted Si.

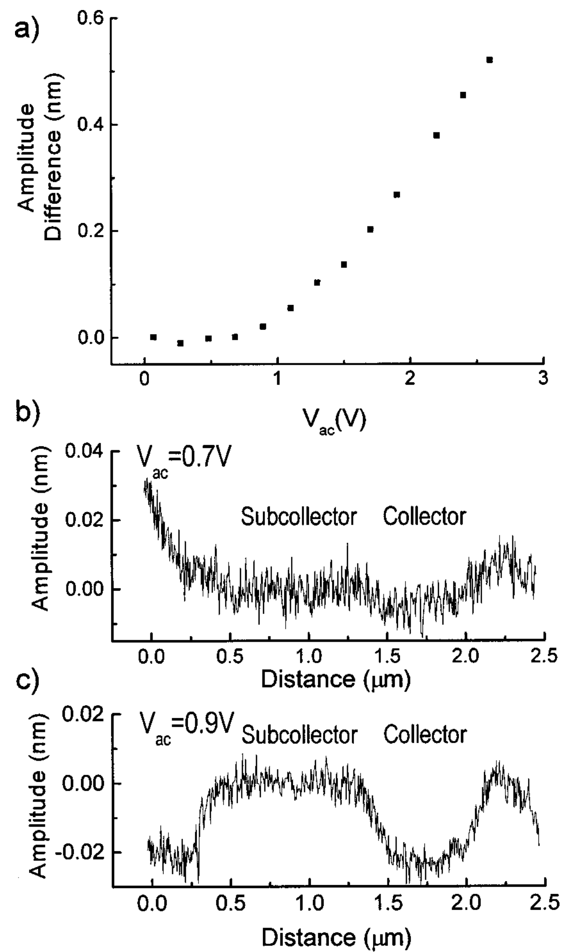

FIG. 3. (a) Capacitive force contrast (amplitude difference) between the collector and subcollector layers of the 120 nm base HBT structure as a function of V_{ac}, at a lift height of 20 nm. (b), (c) Corresponding average line scans of the capacitive force data for (b) $V_{ac}=0.7$ and (c) $V_{ac}=0.9$ V, showing the onset of contrast between the device regions as V_{ac} is increased.

Figure 3(a) shows a plot of the capacitive force contrast (amplitude difference) between the collector and subcollector layers versus V_{ac} for the 120 nm base sample, obtained at a lift height of 20 nm. The experimental uncertainty in each amplitude difference measurement is estimated to be ±0.005 nm or less. For sufficiently small V_{ac} very little contrast is observed, as expected for these conditions since the Fermi level will remain pinned at the exposed semiconductor surface. A threshold voltage V_{th} may be defined as the applied total potential V required to completely empty or fill the surface states. Due to contributions to the total potential from the surface potential difference $\Delta\Phi/q$, the threshold voltage may be asymmetric during the ac voltage cycle. $\Delta\Phi/q$ may also change with applied bias V_{ac} due to tip-induced band bending.[16] However, this change is small in comparison to the maximum amplitude of the applied bias voltage and may therefore be neglected. An additional asymmetry may arise from different electronic state densities in the regions above and below the Fermi level pinning position on the semiconductor surface. Because these additional contributions should be relatively small, the total potential V is therefore approxi-

mated as V_{ac} and we are able to estimate V_{th} from the data shown in Fig. 3.

For $V_{ac} < V_{th}$, electronic states present at the cleaved sample surface can accommodate the charge associated with the electric field between the probe tip and sample. For $V_{ac} \geqslant V_{th}$, the surface charge that would be required to maintain the Fermi level at its pinning position exceeds the surface density of states; the Fermi level therefore becomes unpinned, and contribution of additional charge from accumulation or depletion in the sample leads to tip-induced band bending. This change in capacitive force contrast around V_{th} is evidence that the applied ac modulation frequency ω is sufficient that the semiconductor surface alternates between accumulation and depletion during the ac voltage cycle.

From Fig. 3(a), we see that for sufficiently large values of V_{ac}, the amplitude contrast increases with V_{ac}. The amplitude contrast dependence on V_{ac} is seen to be a combination of the depletion layer width dependence [Eqs. (8) and (9)] and the quadratic dependence of $(dF/dz)_{2\omega}$ on V_{ac} [Eq. (6)]. From the amplitude difference plotted in Fig. 3(a) we find V_{th} is approximately 0.9 V, which allows us to estimate the maximum surface charge that can be present on the cleaved (110) surface. The estimated V_{th} of 0.9 V, combined with the lift height of 20 nm, yields a maximum surface charge density of $\sim 3.9 \times 10^{-8}$ coulombs/cm^2, corresponding to a charged surface state density of $\sim 2.5 \times 10^{11}\,\text{cm}^{-2}$. Xu and Hsu[4] have reported a surface state density for the GaAs (100) surface of $\sim 2 \times 10^{12}\,\text{cm}^{-2}$. Given that the ideal GaAs (110) surface in the absence of defects and contamination is unpinned,[21,22] our estimate of surface state density for a cleaved (110) surface exposed to air appears quite reasonable. A refined estimate of V_{th} to include contributions of V_{dc} and $\Delta\Phi/q$ to the total potential V does not significantly change our estimate of the surface charge density, or the corresponding charged surface state density.

Average line scans of the data from which Fig. 3(a) was derived are presented in Figs. 3(b) and 3(c), for $V_{ac} = 0.7$ and 0.9 V, respectively. At $V_{ac} = 0.7$ V [Fig. 3(b)] there is little amplitude contrast between the collector and subcollector regions and the device layers are not well delineated. For $V_{ac} = 0.9$ V [Fig. 3(c)] however, the collector–subcollector amplitude difference markedly increases and the device layers are clearly revealed.

A plot comparing averaged line profiles derived from capacitive force image data for both the 50 and 120 nm base-width HBT samples is shown in Fig. 4; in both cases data were obtained with $V_{ac} = 2.6$ V and at a lift height of 20 nm, and the same probe tip was used to obtain both scans. The topographic feature associated with the oxidized $Al_xGa_{1-x}As$ emitter layers in each sample was used to identify, and spatially align, the emitter–base (E/B) interface in the two scans, and this interface is taken as the origin on the horizontal axis. In addition, data for the 120 nm base sample were shifted vertically by $+0.21$ nm for clarity. The difference in base width between the two samples is clearly evident. A reference base width in each individual sample was defined to be the separation between the E/B interface and the spatial location corresponding to the midpoint in amplitude contrast between the base and collector region. Detailed

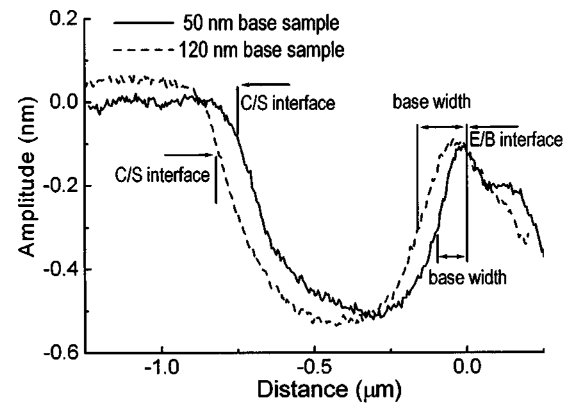

FIG. 4. Capacitive force contrast comparing average line scans for the 50 nm base sample (solid line) and the 120 nm base sample (dashed line). The emitter–base (E/B) interface (set at 0.0 μm) is identified using the surface feature exhibited in Fig. 2(a), and was used to spatially align the scans. Data for the 120 nm base sample were offset vertically by $+0.21$ nm. The collector–subcollector (C/S) interface for each sample is indicated.

analysis and comparison of the amplitude contrast yields a base-width difference of 63 ± 3 nm between the two samples, in excellent agreement with the nominal difference of 70 ± 7 nm. The absolute base-layer widths determined in this manner are wider than expected for each sample, a discrepancy we attribute to depletion layer effects in the vicinity of the base. Nevertheless, these results clearly demonstrate the ability, using the capacitive force imaging technique, to obtain a reliable and precise measure of differences in the base-layer widths between different HBT samples based upon direct measurement of electronic properties.

Figure 4 also highlights once again the dependence of the amplitude contrast on the local dopant concentration in the sample. In each sample the heavily doped base layer is exposed and distinguishable from the more lightly doped n-GaAs collector region. Additionally, the heavily doped n^+-GaAs subcollector regions are distinguished from the more lightly doped n-GaAs collector layers. The nominal collector–subcollector (C/S) interface for each sample is indicated in Fig. 4. As mentioned previously, the 50 nm base sample shows additional amplitude contrast within the collector layers, revealing the variation in dopant concentration (from $N_D = 3 \times 10^{16}$ to $6 \times 10^{16}\,\text{cm}^{-3}$) within the collector layers, and demonstrating sensitivity of the capacitive force imaging technique to a factor of 2 change in local dopant concentration. This is apparent from the asymmetry of the amplitude feature in this region (approximately located between -0.05 and -0.75 μm). In contrast, the collector region of the 120 nm base sample (located between -0.12 and -0.82 μm) contains no such variation in dopant concentration and structure in the amplitude contrast within this collector layer is correspondingly absent.

IV. SUMMARY

We have used a variation of standard electrostatic force microscopy, referred to as capacitive force imaging, in which an ac tip–sample bias voltage is applied and variations in oscillation amplitude of the probe tip in response to the electrostatic force component at frequency 2ω are detected, to

characterize two $Al_xGa_{1-x}As/GaAs$ heterojunction bipolar transistor epitaxial layer structures, one with 50 nm base width and the other with 120 nm base width. Theoretical analysis and experimental results indicate that the amplitude contrast arises from variations in the local capacitance between the tip and sample, and is therefore dependent on the local dopant concentration through variations of the depletion layer depth extending into the sample surface. The contrast obtained yields clear delineation of individual device layers, and enables a precise determination, to within better than 10 nm, of the difference in base-width between the two HBT samples examined. The technique readily distinguishes between regions of the same chemical composition but different dopant concentrations, as demonstrated by the very marked contrast present between the heavily doped subcollector regions and the more lightly doped collector and substrate/buffer regions. Sensitivity to a factor of two difference in dopant concentration has been observed, as demonstrated by the change in amplitude contrast between adjacent collector layers with dopant concentrations of 3×10^{16} and $6\times10^{16}\,cm^{-3}$ in the 50 nm base sample.

ACKNOWLEDGMENTS

P.A.R. thanks K. V. Smith at UCSD for many valuable discussions and P. McPhail and R. Tench at Digital Instruments, Veeco Metrology Group for useful technical discussions. Part of this work was supported by the National Science Foundation (Award No. ECS 95-01469), Rockwell Science Center, and the UC MICRO program. One of us (E.T.Y.) acknowledges financial support from the Alfred P. Sloan Foundation.

[1] T. Mizutani, M. Arakawa, and S. Kishimoto, IEEE Electron Device Lett. **18**, 423 (1997).
[2] H. O. Jacobs, H. F. Knapp, S. Müller, and A. Stemmer, Ultramicroscopy **69**, 39 (1997).
[3] A. K. Henning, T. Hochwitz, J. Slinkman, J. Never, S. Hoffman, P. Kaszuba, and C. Daghlian, J. Appl. Phys. **77**, 1888 (1995).
[4] Q. Xu and J. W. P. Hsu, J. Appl. Phys. **85**, 2465 (1999).
[5] A. J. Howard, O. Blum, H. Chui, A. G. Baca, and M. H. Crawford, Appl. Phys. Lett. **68**, 3353 (1996).
[6] Y. Martin, D. W. Abraham, and H. K. Wickramasinghe, Appl. Phys. Lett. **52**, 1103 (1988).
[7] D. W. Abraham, C. Williams, J. Slinkman, and H. K. Wickramasinghe, J. Vac. Sci. Technol. B **9**, 703 (1991).
[8] T. Hochwitz, A. K. Henning, C. Levey, C. Daghlian, J. Slinkman, J. Never, P. Kaszuba, R. Gluck, R. Wells, J. Pekarik, and R. Finch, J. Vac. Sci. Technol. B **14**, 440 (1996).
[9] Digital Instruments, Veeco Metrology Group, Santa Barbara, CA. Nanoscope, MultiMode, LiftMode, and TappingMode are registered trademarks of Digital Instruments, Veeco Metrology Group.
[10] M. Nonnenmacher, M. P. O'Boyle, and H. K. Wickramasinghe, Appl. Phys. Lett. **58**, 2921 (1991).
[11] R. Wiesendanger, *Scanning Probe Microscopy and Spectroscopy: Methods and Applications* (Cambridge University Press, Cambridge, 1994), Chap. 2.
[12] W. E. Spicer, P. W. Chye, P. R. Skeath, C. Y. Su, and I. Lindau, J. Vac. Sci. Technol. **16**, 1422 (1979).
[13] M. L. O'Malley, G. L. Timp, S. V. Moccio, J. P. Garnp, and R. N. Kleiman, Appl. Phys. Lett. **74**, 272 (1999).
[14] M. L. O'Malley, G. L. Timp, W. Timp, S. V. Moccio, J. P. Garnp, and R. N. Kleiman, Appl. Phys. Lett. **74**, 3672 (1999).
[15] R. Shikler, T. Meoded, N. Fried, B. Mishori, and Y. Rosenwaks, J. Appl. Phys. **86**, 107 (1999).
[16] S. M. Sze, *Physics of Semiconductor Devices* (Wiley, New York, 1981), Chap. 7.
[17] J. L. Ebel, T. E. Schlesinger, and M. L. Reed, in *Electrochemical Synthesis and Modification of Materials Symposia*, edited by P. C. Andricacos, S. G. Corcoran, J.-L. Delplancke, and T. P. Moffat (Materials Research Society, Pittsburgh, PA, 1997), Vol. 451, p. 251.
[18] G. Neubauer, A. Erickson, C. C. Williams, J. J. Kopanski, M. Rodgers, and D. Adderton, J. Vac. Sci. Technol. B **14**, 426 (1996).
[19] V. V. Zavyalov, J. S. McMurray, and C. C. Williams, J. Appl. Phys. **85**, 7774 (1999).
[20] P. De Wolf, T. Clarysse, W. Vandervorst, L. Hellemans, Ph. Niedermann, and W. Hänni, J. Vac. Sci. Technol. B **16**, 355 (1998).
[21] J. R. Chelikowsky and M. L. Cohen, Solid State Commun. **29**, 267 (1979).
[22] R. M. Feenstra and J. A. Stroscio, J. Vac. Sci. Technol. B **5**, 923 (1987).